The Astrophysical Journal, 643:923–931, 2006 June 1

SYNTHESIS OF CO AND CO_2 MOLECULES BY UV IRRADIATION OF WATER ICE–COVERED HYDROGENATED CARBON GRAINS

V. Mennella,[1] G. A. Baratta,[2] M. E. Palumbo,[2] and E. A. Bergin[3]

Received 2005 November 15; accepted 2006 January 30

ABSTRACT

We present the results of UV irradiation with Lyα photons of carbon grains with a water ice cap at 11 K. Formation of CO and CO_2 molecules takes place during irradiation. An estimation of the formation cross section of these molecules by Lyα photons has been obtained from the intensity increase of their infrared stretching bands as a function of the photon fluence. The fraction of carbon in the grains converted to CO and CO_2 by UV photons is 0.06 and 0.05, respectively. The spectral profile of the CO stretching feature and that of the CO_2 bending mode indicate a polar environment for these molecules. On the basis of the present laboratory results and those obtained in previous work on ion irradiation of similar samples, it has been possible to estimate the contribution of polar CO and CO_2 produced on carbon grains by energetic processing to the observed column densities of these molecules for dense clouds whose visual extinction is known. A significant amount of polar CO and CO_2 is produced through the mechanism we have studied. Furthermore, we have found that the laboratory profile of the bending band of CO_2 produced on carbon grains is compatible with that observed toward the field star Elias 16.

Subject headings: astrochemistry — dust, extinction — infrared: ISM: lines and bands — methods: laboratory

1. INTRODUCTION

In recent years, ground-based and space-borne infrared observations have shown that a rich variety of molecules are frozen on dust grains in cold and dense interstellar environments. Carbon dioxide and carbon monoxide are the two most abundant carbon-based molecules present in ice mantles. The abundance of solid CO is highly variable from close to 0% up to 50% relative to H_2O ice. Early studies of the CO stretching profile have shown that two molecular environments, namely, polar and apolar, are present in icy grain mantles (e.g., Kerr et al. 1993; Chiar et al. 1994, 1995; Teixeira et al. 1998). Recently, Pontoppidan et al. (2003) have performed a phenomenological line shape fitting analysis of the CO band of a large sample of low-mass star-forming regions. Three components, named red, medium, and blue and centered at 2136.5, 2139.9, and 2143.7 cm^{-1}, respectively, can be necessary to reproduce the profile of the feature, indicating that three molecular environments of solid CO can exist under interstellar conditions.

Solid CO_2 has extensively been studied with the *Infrared Space Observatory*. It is a widespread component of molecular clouds. It has been observed toward objects with different physical and chemical conditions such as active star-forming regions and quiescent clouds. Its abundance relative to water ice is between 10% and 23% over many lines of sight, with no systematic difference between young stellar objects and background field stars (e.g., Gerakines et al. 1999; Whittet et al. 1998; Nummelin et al. 2001). The *Spitzer* telescope is offering the opportunity to observe the CO_2 bending mode toward faint low-mass stellar objects and field stars. The results obtained confirm that solid CO_2 is an ubiquitous species with abundances that range from 15% to 35% with respect to water ice. Furthermore, the profile of the band indicates that no annealing has occurred toward field stars (Bergin et al. 2005), while the signature of thermal processing is evident toward embedded objects (Boogert et al. 2004).

Understanding the formation and evolution of these molecules is the key issue. Laboratory work on ice analogs has been of fundamental importance to derive the column densities of interstellar CO and CO_2 and to define their physical and chemical properties and evolution. Systematic studies of the infrared spectra of CO_2 and CO-bearing ices and their modifications under thermal processing and irradiation by ions and photons have been carried out (e.g., Sandford et al. 1988; Sandford & Allamandola 1990; Palumbo & Strazzulla 1993; Gerakines et al. 1996; Ehrenfreund et al. 1997; Palumbo & Baratta 2000; Loeffler et al. 2005; van Broekhuizen et al. 2006). On the basis of the laboratory results and modeling of the molecular composition of ice mantles, it is thought that most of the CO present in ice mantles is the result of direct condensation of CO molecules from the gas phase. On the contrary, since the gas-phase abundance of CO_2 is low, its synthesis should occur on grains as a result of energetic processing of ice mantles and/or surface reactions. In the first case, CO_2 forms through reactions of C-bearing molecules (primarily CO) with O atoms coming from the dissociation of other molecules present in the mantles. CO_2 is formed with high efficiency by energetic processing due to UV photons and ions in ice mixtures containing CO and H_2O (e.g., Moore et al. 1991; Ehrenfreund et al. 1997; Palumbo et al. 1998; Watanabe & Kouchi 2002). In the second case, the formation of CO_2 molecules should occur by oxidation of CO molecules of mantles by accreting oxygen atoms. Laboratory studies of CO oxidation by oxygen atoms have not provided univocal results on the activation energy of the process (Fournier et al. 1979; Grim & d'Hendecourt 1986; Roser et al. 2001). Thermal processing should not play any role in the formation of solid CO_2. In fact, carbon dioxide has been detected in cold quiescent regions of the Taurus molecular cloud (TMC) toward the field stars Elias 16 and Elias 13, indicating that it can form without processing by an embedded protostar (Whittet et al. 1998; Nummelin et al. 2001; Bergin et al. 2005). On the other hand, thermal annealing has been considered as the

[1] INAF–Osservatorio Astronomico di Capodimonte, Via Moiariello, 16, 80131 Naples, Italy.
[2] INAF–Osservatorio Astrofisico di Catania, Via S. Sofia, 78, 95123 Catania, Italy.
[3] Department of Astronomy, University of Michigan, 825 Dennison Building, 500 Church Street, Ann Arbor, MI 48109.

driving factor for the evolution of CO_2-bearing ices in star-forming regions (Gerakines et al. 1999).

Recently, the influence of the grain type on the evolution of the composition of ice mantles during energetic processing has been considered. Ion irradiation of carbon grains under simulated dense cloud conditions produces CO and CO_2 molecules (Mennella et al. 2004, hereafter MPB04). The CO_2 produced on carbon grains by cosmic rays contributes in part to the observed CO_2. In the case of CO, the spectral profile and the contribution to the observed column densities indicate that CO produced by cosmic-ray irradiation is a good candidate for the red component of the interstellar band. Moreover, formation of CO and CO_2 has been observed after ion irradiation, with different ions and energies, of water ice deposited on top of several carbonaceous materials at different temperatures (see Gomis & Strazzulla 2005). Chakarov et al. (2001) have reported the production of CO and CO_2, among other species, during UV (5.5 eV) irradiation of H_2O co-adsorbed with alkali metal atoms on graphite at 90 K. Formation of carbon monoxide and carbon dioxide is initiated by hot electron attachment to a metal-water complex determining water-reactive species (e.g., H and OH). In fact, UV photons in their experiments are not absorbed by the water layer; that is to say, these photons can cause neither formation of radicals nor photodissociation.

In this paper, we further investigate this aspect by studying the formation of CO and CO_2 molecules by Lyα irradiation of hydrogenated carbon grains covered with a water ice layer. To quantify the effects of UV irradiation, we have estimated the conversion efficiency of C atoms of carbon grains to CO and CO_2 molecules. The corresponding formation cross sections by Lyα photons have been derived from the intensity increase of the CO_2 and CO stretching bands as a function of the photon fluence. Section 2 contains a description of the production, UV photolysis, and characterization by IR spectroscopy of the samples, while the results and their discussion are reported in § 3. The implications for the evolution of interstellar CO and CO_2 ices are discussed in § 4.

2. EXPERIMENTAL

The experiments of the present work were performed in an ultrahigh vacuum chamber with a base pressure below 1×10^{-9} mbar. At the center of the chamber resides the cold finger of a closed-cycle helium cryostat (Galileo Vacuum model K1). A small resistive heater, operated by a programmable controller, allows the cold finger temperature, measured with a Si thermometer, to be stabilized within 0.1 K or changed from the low-temperature limit to room temperature. The samples are mounted on the cold finger orthogonal to the UV lamp and at an angle of 45° with the IR beam of a FTIR spectrophotometer (Bruker model IFS 66v) to monitor the IR spectral evolution of the samples during irradiation.

2.1. *The UV Lamp*

The UV source of the apparatus is a microwave excited hydrogen flow discharge lamp. It consists of a Pyrex tube with an outer diameter of 10 mm and 1 mm thickness inserted in an Evenson cavity operated at 2.45 GHz. Microwave power is supplied by an Opthos microwave generator (model MPG 4M). The lamp is connected to the vacuum chamber through a MgF_2 window, transmitting photons with $\lambda > 115$ nm. To increase the UV flux a coaxial Al tube is inserted at the end of the lamp (Westley et al. 1995; Baratta et al. 2002).

The UV spectral distribution of the lamp depends on the operating conditions, in particular, on the hydrogen pressure. Lyα (10.2 eV) emission accounts for almost all the UV emission at low pressures ($\lesssim$1 mbar; Westley et al. 1995), while its contribution is less than 5% at higher pressures, where molecular emission with an average energy of 7.4 eV (168 nm) is predominant (Cottin et al. 2003). We operated the source at 0.5 mbar. The pressure has been measured with a capacitance gauge (Balzers model CRT 262). For a given operating condition, the flux varies with time; in addition to short-term fluctuation, a long-term reduction of the intensity is caused by a decrease of the MgF_2 window transmission. Following Baratta et al. (2002), we monitored the flux during sample irradiation by measuring the current generated by photoelectric effect on a platinum wire inserted in the chamber between the source and the sample. To calibrate the wire sensor and measure the photon flux at the sample position, f_{UV}, a platinum foil was placed on the cold finger at the location of the sample, in order to have a foil area irradiated by UV photons equal to that of the sample during measurements. The quantity f_{UV} was derived from the current, i, generated by photoelectrons, from the relation

$$f_{UV} = i/eEA, \quad (1)$$

where e is the electron charge, A is the illuminated area, and E is the photoelectric efficiency of the platinum; E has been measured by Cairns & Samson (1966) in the wavelength range 20–140 nm. Its value is 2.2×10^{-2}, with an error of 20%, for Lyα photons. We could not find any information on the photoelectric efficiency of photons with an energy of 7.4 eV. We measured the ratio of the current on the wire and foil, and using equation (1), we obtained the calibration factor to convert the current (charge) measured with the Pt wire sensor into the flux (fluence) at the sample.

The previous calibration procedure is based on the assumption that the lamp emits only Lyα photons for our operating pressure (Westley et al. 1995). To check this point we inserted a sapphire window into the beam at the end of the lamp. According to the wavelength dependence of the window transmission, it should eliminate the Lyα radiation from the UV beam and transmit part of the photons at longer wavelengths. The insertion of the sapphire window determined a reduction of a factor of $\sim 7 \times 10^2$ of the current generated on the wire sensor and on the Pt foil, indicating that the current is essentially generated by Lyα photons. However, a quantification of the contribution of lower energy photons to the emission is not possible, since the Pt photoelectric efficiency is not known at these energies.

To get more insight into this aspect, we applied the actinometry method using O_2 ice photolysis to form O_3 (e.g., Gerakines et al. 2000; Baratta et al. 2002; Cottin et al. 2003), using the lamp with and without the sapphire window. In both cases we have deposited a tick O_2 ice film, 1.9 and 2.1 μm, respectively, in order to absorb all the UV flux through the ice. The UV flux was evaluated using $A = 1.4 \times 10^{-17}$ cm molecule^{-1} for the absorbance of the O_3 stretching band at 1046 cm^{-1} and a quantum yield QE = 1.92 molecules photon^{-1} for the gas-phase transformation of O_2–O_3. We have obtained $(8.3 \pm 0.9) \times 10^{14}$ and $(2.4 \pm 0.3) \times 10^{13}$ photons cm^{-2} s^{-1} for the two cases. When the sapphire window is present we have taken into account its transmission at 7.4 eV to derive the flux. On the basis of these results we conclude that Lyα (10.2 eV) emission accounts for 97% of the total UV emission of the source for our operating conditions. Moreover, the flux obtained with the actinometry method, $(8.3 \pm 0.9) \times 10^{14}$ photons cm^{-2} s^{-1}, is equal, within the errors, to that measured with the Pt wire sensor, $(1.0 \pm 0.2) \times 10^{15}$ photons cm^{-2} s^{-1}. The UV flux used in each experiment is listed in column (3) of Table 1.

TABLE 1
Lyα Irradiation of Hydrogenated Carbon Grains with a Water Ice Layer at 11 K

Experiment Number (1)	Sample (2)	UV Flux (10^{14} photons cm^{-2} s^{-1}) (3)	N_C (10^{17} cm^{-2}) (4)	d_{H_2O} (nm) (5)	$\tau_{int}(CO_2)$ (cm^{-1}) (6)	$\tau_{int}(CO)$ (cm^{-1}) (7)	N_{CO_2}/N_C (8)	N_{CO}/N_C (9)
First set								
1	ACARL_H_11_W	8.5	7.8	10	0.46	0.04	0.008	0.005
2	ACARL_H_12_W	10.2	10.5	25	1.30	0.14	0.016	0.012
3	ACARL_H_13_W	9.1	11	42	1.58	0.09	0.019	0.007
Second set								
4	ACARL_H_14_W	8.7	2.4	27	0.88	0.18	0.048	0.068
5	ACARL_H_15_W[a]	9.5	1.6	26	0.61	0.14	0.050	0.080
6	ACARL_16_W[a]	6.3	1.6	26	0.48	0.07	0.040	0.040
7	ACARL_H_17_W	4.7	1.6	27	0.70	0.11	0.058	0.063

[a] In this experiment $H_2^{18}O$ was deposited on grains. The intensity and the corresponding column density of the CO and CO_2 bands refer to the sum of the components; see text.

It is worth noting that the use of Lyα photons in the present work should be regarded as representative of FUV irradiation in clouds. The results of our experiments do not depend on that specific FUV wavelength.

2.2. *The Samples*

The irradiation experiments were aimed at simulating UV processing of carbon grains under dense medium conditions. The hydrogenated carbon samples considered in the present research (hereafter ACARL_H) have been described in detail elsewhere (Mennella et al. 2002; MPB04); therefore, only a brief description of their properties is given here. The samples are characterized predominantly by chainlike aggregates composed of spherical grains with an average diameter of 10 nm. They have an absorption coefficient per mass unit at 3.4 μm, K (3.4 μm), of 1.6×10^3 cm^2 g^{-1}, a hydrogen to carbon atom ratio, H/C, of 0.64, and a density of C$-$H bonds per mass unit, n_{CH}, of 3.1×10^{22} bonds g^{-1}. The high degree of hydrogenation was obtained by exposing to an atomic hydrogen beam hydrogen-free carbon grains (hereafter ACARL) produced by laser ablation of carbon targets in a 10 mbar argon atmosphere. The production method simulates hydrogenation of carbon particles by H atoms, likely the key mechanism to explain the presence of aliphatic C$-$H bonds in the diffuse interstellar medium (ISM; Mennella et al. 2002). They reproduce the interstellar C$-$H stretching and bending features (Pendleton & Allamandola 2002) and require the lowest amount of carbon among the analogs studied so far to reproduce the intensity of the interstellar aliphatic features. The samples are also slightly oxidized, probably due to air exposure during the phases of production and analysis (Mennella et al. 1999). The oxygen to carbon atom ratio as deduced from the carbonyl band is 0.03, completely compatible with oxidation of carbon grains in the diffuse ISM (Pendleton & Allamandola 2002). The column density of C atoms of the samples, N_C, has been derived from the optical depth of the 3.4 μm band using K (3.4 μm) and H/C for ACARL_H reported above. It is listed in column (4) of Table 1. The error on this quantity is about 15%, mainly due to the uncertainty on K (3.4 μm).

To reproduce the icy mantle present on grains in dense regions, a water ice layer was deposited on carbon grain samples at 11 K. The mantle thickness of interstellar ices cannot be directly deduced from observations, and its determination is model dependent. A typical value of 25 nm is usually adopted (e.g., Greenberg 1982). We have used this thickness as a reference value in the present work. However, larger and smaller values (set 1 of Table 1) have been considered. Layers of 25 and 40 nm thick have also been considered in ion irradiation experiments of hydrogenated carbon grains with an ice cap (MPB04).[4] The thickness, d_{H_2O}, of the ice layer deposited on carbon grains has been derived from the 3 μm band, using a band absorbance of 2×10^{-16} cm molecule^{-1} (Allamandola et al. 1988) and a density of 1 g cm^{-3}. It is reported in column (5) of Table 1. We add the letter W to the label identifying hydrogenated carbon grain samples, to refer to ice-capped samples.

3. RESULTS AND DISCUSSION

The samples were irradiated with Lyα photons with fluences, F_{UV}, in the range (5×10^{17})–(1×10^{19}) photons cm^{-2}. The maximum photon fluence was 1×10^{19} photons cm^{-2} for all the considered samples, with the exception of ACARL_H_11_W (6×10^{18} photons cm^{-2}). The evolution of the transmittance spectrum with UV fluence has been studied with a resolution of 2 cm^{-1} in the range 4000–1250 cm^{-1}, using a CaF beam splitter.[5] In Figure 1 we report the spectra of ACARL_H_12_W, normalized to that before irradiation, after an intermediate UV fluence and after the maximum processing.

As a result of UV irradiation the intensity of the O$-$H stretching band of water at 3280 cm^{-1} decreases. A similar trend is observed for the aliphatic C$-$H stretching modes of the CH_2 and CH_3 functional groups at 2950, 2925, and 2860 cm^{-1} and for the associated C$-$H bending modes at 1457 and 1378 cm^{-1}. UV irradiation also reduces the intensity of carbonyl groups at 1748 and 1710 cm^{-1}. The intensity decrease of the features of water and carbon grains is accompanied by the appearance in the spectrum of the CO and CO_2 stretching bands, which develop during irradiation. Their intensity at the end of irradiation is reported in columns (6) and (7) of Table 1. The peak position of the CO_2 stretching mode remains stable, within 1 cm^{-1}, at 2339.5 cm^{-1} with a full width at half-maximum (FWHM) of 14 cm^{-1}. The CO stretching band falls, within 1 cm^{-1}, at 2136.5 cm^{-1}, with a FWHM of 13 cm^{-1}, beside the C $\equiv$ C stretching band at 2110 cm^{-1}. The latter band is related to processing of carbon grains; it also

[4] In Table 1 of MPB04 the values of the ice thickness not corrected for the factor, which takes into account the oblique incidence of the IR beam, are erroneously reported.

[5] Due to the bad functioning of the KBr beam splitter, we could use it only in experiment 1.

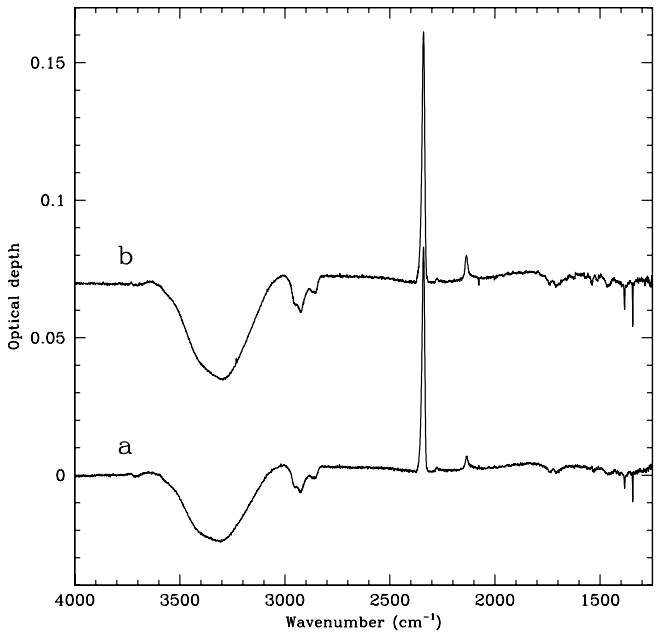

FIG. 1.—Spectra of ACARL_H_12_W after UV irradiation at fluences of (*a*) 5×10^{18} and (*b*) 1×10^{19} photons cm^{-2}. The spectra are normalized to that before irradiation and are offset from each other in ordinates for the sake of clarity.

appears in the spectrum of hydrogenated carbon grains after ion irradiation at room temperature (Mennella et al. 2003). In general, the spectral variations induced by UV processing are similar to those produced by ion bombardment. In the case of experiment 1, the spectral evolution has been studied in a range wider than that of the other experiments, down to 580 cm^{-1}, allowing the detection of the CO_2 bending mode. The band is centered at 657 cm^{-1} and exhibits clear asymmetry, as one can see in Figure 5, where we have reported the average profile of the bands corresponding to the four highest fluences considered in this experiment.

A typical problem of UV processing of ices is the appearance of the stretching bands of CO_2 and CO in the IR spectrum due to contamination (e.g., Gerakines et al. 1996; Munoz et al. 2001; Loeffler et al. 2005). Their intensity depends on the specific conditions of the experimental setup. To evaluate the contribution of the contamination in our spectra, we have performed blank experiments. After each irradiation experiment of grains, we carried out a control experiment depositing a water ice layer, with the same thickness as that present on carbon grains, on a CsI substrate and irradiated for the same fluences. The CO_2 stretching band is present in the spectrum, while CO has not been detected. As an example, we compare the spectrum of ACARL_H_12_W with that of the corresponding blank experiment for the same UV fluence in Figure 2. In our analysis of the formation of CO_2 on carbon grains, for each considered UV fluence, we have subtracted to the observed CO_2 band intensity that obtained in the corresponding blank experiment. At the maximum fluence, contamination accounts for at most 16% of the total CO_2. Although a not negligible amount of spurious CO_2 forms in our experiments, it is very small when compared with that produced during UV irradiation of ices at higher background pressure. For instance, we have found that, for the same fluence, the amount of spurious CO_2 in our experiments is a factor of $\sim$20 lower than that reported by Loeffler et al. (2005) during Lyα irradiation of CO ice at a pressure $\lesssim 10^{-7}$ mbar.[6]

[6] In order to avoid interference with contaminating CO_2, these authors used ^{13}CO to study the effects of energetic processing of carbon monoxide.

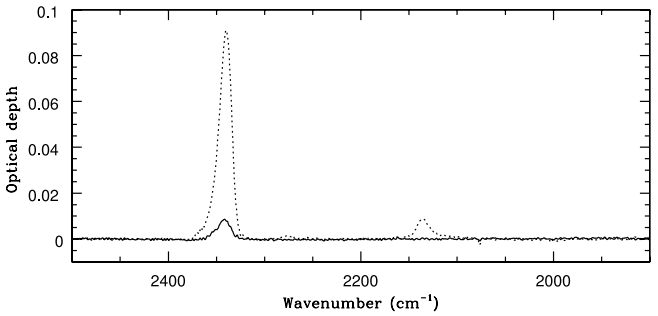

FIG. 2.—Comparison of the spectrum of ACARL_H_12_W (*dashed line*) with that obtained with the corresponding blank experiment (*solid line*). The spectra refer to a UV fluence of 1×10^{19} photons cm^{-2}.

We also carried out an irradiation experiment (number 5 in Table 1) using water isotopically labeled with ^{18}O. The fraction of $H_2^{18}O$ molecules of the liquid water (provided by Aldrich) was 97%. We deposited a $H_2^{18}O$ layer of 26 nm on the sample ACARL_H_15 and irradiated up to a fluence of 1×10^{19} photons cm^{-2}. The spectrum after the maximum irradiation is shown in Figure 3. Two bands are present at 2308 and 2326 cm^{-1}, due to the asymmetric stretching mode of $^{18}O^{12}C^{18}O$ and $^{16}O^{12}C\ ^{18}O$, respectively, with a shoulder at 2340 cm^{-1} due to $^{16}O^{12}C^{16}O$. The $^{12}C^{18}O$ mode at 2090 cm^{-1} develops beside the $^{12}C^{16}O$ feature. Gaussian line shape fitting analysis has been used to determine the integrated intensity of all these components. The intensity ratio of the $^{12}C^{18}O$ and $^{12}C^{16}O$ bands is 1 at the maximum fluence. The corresponding blank experiment with $H_2^{18}O$ indicates that spurious $^{16}O^{12}C\ ^{18}O$ and $^{18}O^{12}C^{18}O$ form with a ratio 1:2.5 (see Fig. 3). They account for 9% and 19% of the corresponding bands of experiment 5. Taking into account the spurious CO_2, the intensity ratio of the $^{16}O^{12}C^{16}O$ and $^{16}O^{12}C^{18}O$ bands with respect to the $^{18}O^{12}C^{18}O$ band is 0.36 and 1, respectively. These intensity ratios are a factor of 6.2 and 1.9 lower than the corresponding values obtained after the maximum fluence in ion irradiation experiments (MPB04). As in the case of ion irradiation, the formation cross sections of the CO and CO_2 components

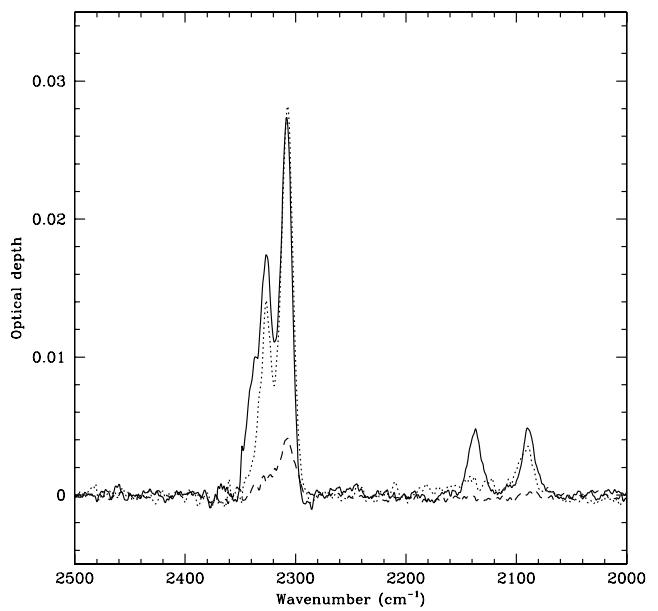

FIG. 3.—CO and CO_2 components of ACARL_H_15_W (*solid line*) and ACARL_16_W (*dotted line*) after the maximum fluence. The spectrum of the blank experiment with $H_2^{18}O$ (*dashed line*) is also shown.

due to the stretching of C with ^{16}O are larger than the corresponding stretching with ^{18}O (see Fig. 5 in MPB04).

According to the purity of the water we used, one expects only a minor contribution of the bands containing ^{16}O. In the case of ion irradiation, MPB04 considered two possible causes for the observed behavior: the presence of $H_2^{16}O$ in the gas deposition system and deposition of residual $H_2^{16}O$ in the background gas. In the present experiments the first cause should be excluded, since UV irradiation experiments of hydrogenated carbon grains with a layer of $H_2^{16}O$, successive to those where $H_2^{18}O$ had been used, did not show the presence of the CO and CO_2 band due to the stretching of C with ^{18}O. We also exclude the second possibility, since we have checked that no detectable deposition of water takes place for a time period corresponding to that of a UV irradiation experiment. The source of ^{16}O should be the carbon grains, which are slightly oxidized. In order to verify this hypothesis, we performed another experiment using $H_2^{18}O$. To reduce as much as possible oxidation of carbon grains due to air exposure during the phases of production and spectroscopic analysis, we did not expose the ACARL_16 sample to hydrogen. In addition, the sample was irradiated with 2×10^{18} photons cm^{-2} before the deposition of the $H_2^{18}O$ layer. The CO and CO_2 bands after the maximum irradiation of 9×10^{18} photons cm^{-2} are compared with those of the experiment 5 in Figure 3. The $C^{16}O$ and $^{16}O^{12}C^{16}O$ bands are absent, while the intensity of $^{16}O^{12}C^{18}O$ feature is reduced of a factor of 0.32 with respect to that of experiment 5. This result indicates that oxygen in carbon grains can account for about 50% and 40%, respectively, of the produced CO and CO_2.

In order to apply the results of our experiments to dense clouds, we have to evaluate the formation cross section, σ, and the conversion factors of C atoms of grains to CO and CO_2 molecules. Within the limits of validity of a first-order approach, the evolution with F_{UV} of the integrated optical depth, τ, of a band is

$$\tau(F_{UV}) = A(1 - e^{-\sigma F_{UV}}) + Be^{-\sigma F_{UV}}, \quad (2)$$

where A is the asymptotic value for the band intensity and B is the initial value. In our experiments the CO and CO_2 stretching bands are absent before irradiation, so that equation (2) becomes

$$\tau(F_{UV}) = A(1 - e^{-\sigma F_{UV}}). \quad (3)$$

We have estimated σ by fitting equation (3) to the observed increase of τ with F_{UV}. The best fits are shown in Figure 4 for ACARL_H_14_W, while the best-fit parameters are listed in Table 2. For the first set of experiments, which refer to samples with the same amount of carbon grains (within the errors) and variable thickness of the water ice layer, σ of CO_2 decreases with d_{H_2O}, while the asymptotic value increases. On the other hand, A and σ are constant (within the errors) in the case of CO. The best-fit parameters of experiment 2, with the exception of A of CO_2, fall within the range of the corresponding values of the second set of experiments, which refer to samples with the same water ice thickness and reduced N_C. The weighted averages of σ for all the samples with an ice thickness of 25 nm are $(3.7 \pm 0.1) \times 10^{-19}$ and $(1.1 \pm 0.1) \times 10^{-19}$ cm^2, respectively, for CO_2 and CO.

The column densities, N_{CO} and N_{CO_2}, obtained at the end of each experiment, normalized to N_C, are reported in columns (8) and (9) of Table 1; N_{CO} and N_{CO_2} have been derived using, as a reference band absorbance, the values of 1.1×10^{-17} and 7.6×10^{-17} cm $molecule^{-1}$ for the CO and CO_2 stretching modes, respectively (Jiang et al. 1975; Yamada & Person 1964; Gerakines et al. 1995). MPB04 have noted that the conversion factors evaluated in this way should be regarded as lower limits. In fact, N_C refers to all C atoms of the grain sample, while only those at the grain water interface should be involved in the formation of CO and CO_2. To reduce this underestimation we have reduced the amount of carbon grains in the second set of experiments. The reduction of N_C has been on average a factor of 5.8 with respect to experiment 2. The corresponding increase of the conversion factors has been on average 5.9 and 3, respectively, for CO and CO_2. This result and the compatibility of the cross sections of experiment 2 with those of the second set of experiments indicate that the formation of CO and CO_2 molecules take places mainly at the grains-water interface. In the second set of experiments, the average ratio of C atoms in CO and CO_2 molecules is 1.3, while their average sum normalized to carbon of grains is 0.11. Therefore, UV photons transform 6% and 5% of the C atoms of carbon grains to CO and CO_2 molecules, respectively. It is worth noting that, due to technical difficulties, we have not studied samples with N_C lower than that considered in the second set of experiments. Therefore, we cannot exclude a possible underestimation of the conversion factors. Irradiation of water ice–covered hydrogenated carbon grains with 30 keV He^+ ions transforms 3% and 2% of C atoms of grains to CO and CO_2 molecules, respectively (MPB04). In that case, however, the average N_C of the samples was 5.6×10^{17} atoms cm^{-2}, 3 times larger than that of the second set of the experiments. The conversion factors should be multiplied by such a factor to normalize them to the same N_C of the samples of the second set of experiments.

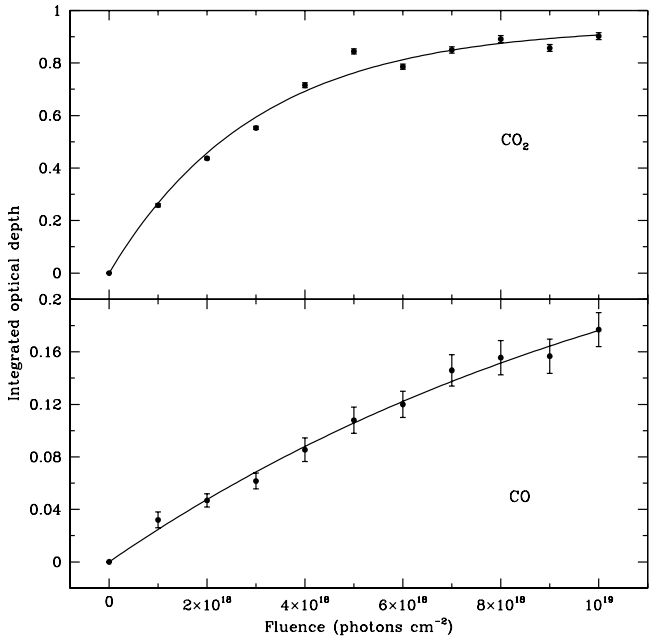

FIG. 4.—Evolution with UV irradiation of the intensity of the CO_2 and CO stretching bands of ACARL_H_14_W. The fits of eq. (3) to the experimental data are also shown. The circles represent the averages, with their standard errors, of several integrations of the band profile resulting from different choices of the baseline.

The discussion of the previous results in terms of all the possible reactions involved in the formation of CO and CO_2 molecules during UV irradiation is out of the aim of the present work. Here we only report some considerations to interpret the observed trends and compare the results with those obtained in previous work on energetic processing of carbon species in the

TABLE 2
CO and CO_2 Formation Cross Sections

Experiment Number	Sample	CO_2		CO	
		σ (10^{-19} cm^2)	A (cm^{-1})	σ (10^{-19} cm^2)	A (cm^{-1})
		First set			
1	ACARL_H_11_W	5.6 ± 0.7	0.51 ± 0.02	0.6 ± 0.3	0.14 ± 0.07
2	ACARL_H_12_W	3.5 ± 0.1	1.36 ± 0.02	0.9 ± 0.2	0.23 ± 0.04
3	ACARL_H_13_W	2.4 ± 0.2	1.80 ± 0.05	0.7 ± 0.3	0.19 ± 0.07
		Second set[a]			
4	ACARL_H_14_W	3.3 ± 0.3	0.94 ± 0.03	0.8 ± 0.2	0.32 ± 0.05
5	ACARL_H_15_W[b]	4.3 ± 0.2	0.63 ± 0.01	2.2 ± 0.3	0.16 ± 0.01
7	ACARL_H_17_W	4.1 ± 0.2	0.70 ± 0.01	1.0 ± 0.2	0.17 ± 0.02

[a] Best fit to the data of experiment 6 has not been performed due to the poor sampling of the band intensities as a function of F_{UV}.
[b] In this experiment $H_2^{18}O$ was deposited on grains. The parameter A and the cross section refer to the sum of the CO and CO_2 band components; see text.

presence of water. In general, formation processes of a molecular species during irradiation can be accompanied by processes that tend to destroy the formed species. This is certainly true in the case of energetic processing of C-bearing molecule ice. For instance, CO_2 forms after UV irradiation of CO in a water ice matrix (e.g., Watanabe & Kouchi 2002); however, photodestruction of CO_2 embedded in water is also observed (e.g., Cottin et al. 2003). Within the limits of validity of a first-order approach, when two competitive processes are active, the parameters A and σ of equation (3) are

$$A = \frac{\tau_m \sigma_f}{\sigma}, \quad \sigma = \sigma_f + \sigma_d, \tag{4}$$

where τ_m is the maximum band intensity if destructive processes were absent and σ_f (σ_d) is the formation (destruction) cross section; it is the sum of the cross sections of all the different chemical reactions that form (destroy) the considered species. It should be noted that in our samples the maximum band intensity or, equivalently, the maximum column density, N_m, for CO and CO_2 are unknown.[7]

The decrease of σ of CO_2 observed in the first set of experiments is a consequence of the increase of the absorption of the water ice layer. In fact, the fluence at the carbon grains-water layer is $F_{UV,\,in} = F_{UV} e^{-\alpha d_{H_2O}}$, where F_{UV} is the fluence incident on the sample and α is the absorption coefficient of amorphous water ice. Assuming as a reference the cross section (σ_1) and the water ice thickness ($d_{H_2O,1}$) of the first experiment, we have $\sigma/\sigma_1 = e^{-\alpha(d_{H_2O} - d_{H_2O,1})}$. With this relation the values obtained in the other two experiments are reproduced, within 5%, using $\alpha = 28$ cm^{-1} for Lyα photons (Baratta et al. 2002). Therefore, the cross section per incident photon at the interface grains-water is constant with increasing d_{H_2O}. Consequently, the observed increase of A for CO_2 with d_{H_2O} implies an increase of $\tau_m \sigma_f$.[8] We note that, although we cannot exclude a marginal contribution to the formation of CO and CO_2 through water-reactive species produced by hot electron as in the experiment by Chakarov et al. (2001) mentioned in § 1, our previous discussion of the observed trends with varying water ice layers indicates that photolysis of water molecules is the driving production mechanism in our experiments.

In the case of CO, the constant value of σ implies an increase of the cross section and, again, an increase of $\tau_m \sigma_f$, since the asymptotic value A increases with d_{H_2O}. In both cases the initial formation yield is larger for thicker water ice layers. This result can be interpreted in terms of an increase of radicals such as OH, O produced by photons in the water ice, and it suggests diffusion of the radicals on a length scale of a few tens of nanometers. As noted above, the parameters A and σ of CO of experiment 2 are compatible with the dispersion of the corresponding values of the second set of experiments. This result implies that, keeping constant the thickness of the water ice layer, the reduction of N_C does not influence the initial formation yield. On the contrary, in the case of CO_2, A decreases by a factor of 1.8, while σ does not change, indicating a decrease of the initial formation yield. The origin for the different behavior is not clear, and further work is necessary to clarify this aspect.

The cross sections estimated in the present work, $(3.7 \pm 0.1) \times 10^{-19}$ and $(1.1 \pm 0.1) \times 10^{-19}$ cm^2, for CO_2 and CO, respectively, are 3 orders of magnitude lower those obtained after 30 keV He^+ ion irradiation of ACARL_H_W, 7.5×10^{-16} cm^2. The difference is due to the different interaction of photons and ions with solids (see Johnson [1990], Moore [1999], and [MPB04] for details). It is worth noting that, although the formation cross section by UV photons are smaller than those by ions, the corresponding formation rates are comparable in dense clouds, since the estimated UV flux is larger than the cosmic-ray flux (see § 4). In addition to the difference of the absolute values, we note a difference in the relative values of the cross sections. The ratio of the CO_2 and CO cross sections is 1 and 3.5, respectively, for ion and UV irradiation. This reflects the different formation and destruction cross sections of CO and CO_2 after ion and UV irradiation, as discussed by Loeffler et al. (2005).

Finally, we compare σ of CO_2 with that obtained from energetic processing of CO ice in a water matrix. MPB04 have derived a cross section of 1.4×10^{-18} cm^2 from the rate reported by Watanabe & Kouchi (2002) for the formation of CO_2 in a H_2O:CO = 10:1 mixture at 12 K after UV processing. This value is a factor of 3.8 larger than the cross section obtained in the present work for ACARL_H_W. Similarly, a factor of 3 was found for the CO_2 cross section from 30 keV He^+ ion irradiation of a H_2O:CO = 10:1 mixture and ACARL_H_W (MPB04).

[7] In simpler cases, such as ion or UV irradiation of optically thin film of CO ice, N_m is known. For CO_2, N_m is half of the initial column density of CO molecules.
[8] The quantity $\tau_m \sigma_f$ is proportional to the initial formation yield.

TABLE 3
CO AND CO_2 ICE COLUMN DENSITIES

Line of Sight	A_V	N_{CO} (obs)[a]	N_{CO} (eq. [10])	N_{CO_2}(obs)	N_{CO_2} (eq. [10])	Reference
Elias 13 (TMC).....	11.2	0.9 (−)	0.56	2.1	0.73	1, 2
Elias 16 (TMC).....	23.3	6.8 (1.2)	1.40	5.0	1.84	1, 3
Elias 18 (TMC).....	18.5	2.7 (1.1)	1.07	5.2	1.40	1, 2
HH 100-IR (R CrA).....	25	7.0 (2.5)	1.52	6.2	2.00	2, 4, 5
RAFGL 989.....	25	4.3	1.52	8.1	2.00	2
Elias 29 (ρ Oph).....	11	1.6 (0.3)	0.27	6.7	0.37	6, 7

NOTE.—The column densities are in units of 10^{17} cm^{-2}.
[a] The values in parentheses refer to the polar component.
REFERENCES.—(1) Chiar et al. 1995; (2) Nummelin et al. 2001; (3) Bergin et al. 2005; (4) Pontoppidan et al. 2003; (5) Whittet et al. 1996; (6) Gerakines et al. 1999; (7) Kerr et al. 1993.

The difference can be attributed to different relative distributions of carbon and oxygen atoms in the samples considered in the two cases: CO molecules embedded in an H_2O matrix and carbon grains with a water layer.

4. ASTROPHYSICAL IMPLICATIONS

The present experiments show that, as in the case of ion irradiation, CO and CO_2 molecules can directly form from carbon of carbon grains during UV irradiation of carbon grains with a water ice layer. Therefore, this formation mechanism regards, in general, energetic processing of carbon grains under simulated interstellar dense medium conditions. In order to evaluate its contribution to the observed column density of CO and CO_2 in dense clouds, we apply the model outlined by MPB04 in the case of cosmic-ray irradiation. It relies on three points: (1) the estimation of the column density of C in carbon grains, N'_C, in dense regions as a function of the visual extinction of the cloud A_V; (2) the use of the experimental values as representative of the conversion of C atoms of carbon grains to CO and CO_2 in dense clouds; and (3) the estimate of the transformation rate to evaluate the amount molecules formed during the cloud lifetime of 3×10^7 yr.

The time evolution of the column density of the CO and CO_2 molecules produced on carbon grains by cosmic rays and UV photons is

$$N(t) = N_A(1 - e^{-Rt}), \tag{5}$$

where the rate, $R = R_{UV} + R_{CR} = \sigma_{UV}\Phi_{UV} + \sigma_{CR}\Phi_{CR}$, is the sum of the formation and destruction rates due to photons and cosmic rays, and

$$N_A = \frac{R_{f,UV}N_{A,UV} + R_{f,CR}N_{A,CR}}{R} \tag{6}$$

is the weighted average of the corresponding asymptotic values, the weights being the rates. The quantity $N_{A,UV}$ ($N_{A,CR}$) is the asymptotic value (see eq. [4]) if cosmic-ray (UV) irradiation were absent. To estimate R_{UV} we have considered only the internal UV field induced by cosmic-ray fluorescence of molecular hydrogen. Using the value of $\Phi_{UV} = 4.8 \times 10^3$ photons cm^{-2} s^{-1} (Mennella et al. 2003) and the formation cross sections of the present work, we obtain 5.3×10^{-16} and 1.8×10^{-15} s^{-1}, respectively, for the formation rate of CO and CO_2. The corresponding value for cosmic rays is 2.4×10^{-16} s^{-1} for both CO and CO_2 (MPB04). To evaluate N_A we use the conversion factors of C carbon of grains to CO and CO_2 and the column density of carbon in carbon grains,

$$N'_C = 2.1 \times 10^{17} A_V, \tag{7}$$

estimated by MPB04. This value corresponds to 115 ppm of carbon relative to hydrogen locked in carbon grains (see [MPB04] for more details). The present experiments indicate that when carbon grains are covered with a water ice layer, about 6% and 5% of the C atoms of the grains are transformed, respectively, to CO and CO_2 molecules at the end of UV irradiation. In the case of ion irradiation, the corresponding values, once normalized to the same N_C of the samples considered in the second set of experiments of the present work (see § 3), are 9% and 6%. With the previous values we obtain for the time evolution of column density of CO and CO_2 produced on carbon particles,

$$N_{CO} = 1.3 \times 10^{16}(1 - e^{-7.7 \times 10^{-16} t})A_V,$$
$$N_{CO_2} = 1.1 \times 10^{16}(1 - e^{-2.0 \times 10^{-15} t})A_V. \tag{8}$$

For $t = 3 \times 10^7$ yr, the dense cloud timescale, we have

$$N_{CO} = 7.0 \times 10^{15} A_V, \quad N_{CO_2} = 9.3 \times 10^{15} A_V. \tag{9}$$

We note that the formation of CO and CO_2 molecules by energetic irradiation of carbon grains requires the presence of ice mantles on carbon grains. It is well known that there is an extinction threshold, A_{th}, above which water ice is detected on grains within a cloud. We have taken into account this observational constraint by introducing a threshold for the water ice in equation (9):

$$N_{CO} = 7.0 \times 10^{15}(A_V - A_{th}), \quad N_{CO_2} = 9.3 \times 10^{15}(A_V - A_{th}). \tag{10}$$

The uncertainty on the estimated column densities is about 30%, excluding that on A_V and A_{th}. For clouds with known A_V, the column densities obtained from equation (10) are reported in Table 3 with the corresponding observed quantities. The considered lines of sight are the same as those of Table 3 of MPB04. We have updated the values relative to Elias 16 (TMC), adopting those reported by Bergin et al. (2005). For Elias 29 (ρ Oph) we have used $A_V \sim 11$ mag. The value $A_V = 48$ mag used in MPB04 refers to total extinction along the line of sight. However, as indicated by the analysis of this line of sight, the visual extinction of the foreground clouds where most of the ices should be present is $\sim$11 mag (Boogert et al. 2002). In the case of HH 100-IR, we have reported the more recent CO values obtained by Pontoppidan et al. (2003). For some clouds we have also listed in Table 3 the column densities for the polar component of CO. The polar column densities have been revalued using a band absorbance of 1.1×10^{-17} cm molecule^{-1} for the CO diluted in water (Gerakines et al.

1995) instead of 1.7×10^{-17} cm molecule^{-1} used in the original papers listed in Table 3. Since the work by Gerakines et al. (1995) the lower value has been adopted for the polar component. We also used that value to estimate N_{CO} in equation (10). Concerning the extinction threshold for H_2O ice in equation (10), we have used $A_{th} = 3.2$ mag for the three lines of sight of the TMCs and for HH 100-IR in R CrA (Chiar et al. 1995; Whittet et al. 1996) and $A_{th} = 7$ mag for Elias 29 in ρ Oph (Shuping et al. 2000). For RAFGL 989 we also used a extinction threshold of 3.2 mag.

The comparison of Table 3, excluding Elias 13 (see below), indicates that the synthesis of CO by energetic processing of carbon grains accounts for 15%–40% of the observed solid CO. This compares well with the range 10%–60%, estimated by MPB04, for the ratio of the red component to the total observed CO of the sample of low-mass star-forming clouds of Pontoppidan et al. (2003). However, CO produced by UV and ion irradiation on carbon grains shows a polar character, as indicated by the peak position and width of the stretching feature. Therefore, limiting the comparison to that component, one can see that our model accounts for the totality of the observed polar CO in Elias 16, Elias 18, Elias 29, and a significant fraction in the case of HH 100-IR, while an overproduction is observed for Elias 13. Chiar et al. (1995) noted that the absence of a polar component in the spectrum of Elias 13 is unusual and could be a result of the low signal-to-noise ratio of the spectrum and/or the presence of gas-phase CO lines. As one can see in Table 3, CO_2 produced by energetic processing of water ice–coated carbon grains accounts for between 6% and 37% of the total column densities for the considered clouds. Contrary to what was concluded in MPB04, the formation of carbon dioxide on carbon grains is significant. The reduction of the underestimation of the conversion factors of C atoms of grains and the inclusion of UV processing in the evaluation of the molecules produced in dense clouds are the reasons for revising our earlier conclusion.

The lines of sight toward field stars located behind quiescent clouds are useful to constrain the origin of CO_2, since processing by an embedded source can be excluded (Whittet et al. 1998; Nummelin et al. 2001). The bending mode of CO_2 is more sensitive than the stretching feature to the ice composition (Ehrenfreund et al. 1996, 1997). The first *Spitzer* observations of the 15.2 μm bending mode of CO_2 toward field stars reported by Bergin et al. (2005) represent a unique resource to study the formation mechanisms of CO_2. Among the clouds observed by these authors, the signal-to-noise ratio of the spectrum of Elias 16 allowed them to analyze the CO_2 band on the basis of laboratory interstellar ice analogs. To reproduce the profile of CO_2 bending mode, two components are necessary: a broad component consistent with solid CO_2 within a polar water ice and a narrow band due to CO_2 embedded in an apolar matrix. The polar component accounts for 85% of the band intensity. Fractions of polar CO_2, comparable to that obtained by Bergin et al. (2005), have been reported by Knez et al. (2005) from the analysis of other *Spitzer* spectra of Elias 13 and Elias 16 and of the other field star CK 2 in the Serpens cloud, despite the use of different ice mixtures.

To check the spectral compatibility of CO_2 produced in our experiments with that observed toward field stars, we use the spectrum of Elias 16 from Bergin et al. (2005). In Figure 5 we report the fit to the Elias 16 bending mode obtained using the CO_2 profile of the present work for the polar component and the profile of CO_2 produced after ion irradiation with 200 keV H^+ of CO ice at 16 K for the apolar component. These profiles are in optical depth units and do not take into account grain shape effects. As discussed by Loeffler et al. (2005), an amount of a few percent of the observed interstellar solid CO_2 can be formed after processing of CO-rich icy mantles. The comparison of the observed CO_2 bending mode with laboratory spectra of ion-irradiated ice mixtures will be discussed in a forthcoming paper. Our fit shows that CO_2 produced on carbon grains is a good spectroscopic analog of the interstellar polar component. Moreover, using our laboratory band profiles, the fit indicates that the polar component accounts for 93% of the total intensity, in agreement with the results of Bergin et al. (2005) and Knez et al. (2005). It is worth noting that the fit of Figure 5 was performed without any constraint on the amount of the polar component. However, our modeling indicates that CO_2 produced by energetic processing of carbon grains with a water ice cap can account for 37% of the observed column density in the case of Elias 16 (see Table 3). Further work is necessary to understand if, once the contribution of additional mechanisms that form polar CO_2 has to be evaluated, this difference is due to a possible underevaluation of the contribution of CO_2 formed after processing of mantled carbon grains, as discussed below. Our results indicate that energetic processing could contribute to the formation of both polar and apolar CO_2. In particular, polar CO_2 would mainly be produced on carbon grains when water ice mantles are formed, and this agrees with the observation that the CO_2 extinction threshold is close to that of water ice. Apolar CO_2 would form when freeze-out of gas-phase CO takes place. This is an alternative scenario with respect to that proposed by Bergin et al. (2005), who considered that solid CO_2 is formed after grain surface reactions and suggested that polar CO_2 forms along with water ice after oxidation of CO and hydrogenation of oxygen, while apolar CO_2 forms after CO oxidation in the outer part of the cloud rich in atomic oxygen. An ongoing study (Pontoppidan et al. 2005) on the spatial distribution of ices in dark cloud cores shows that the abundance of water ice is almost constant in most dark cloud environments, while abundance of CO ice strongly depends on the density; the abundance of CO_2 ice moderately depends on the density. These results indicate that a formation route must exist for CO_2 before CO accretion occurs. Our modeling shows a possible route.

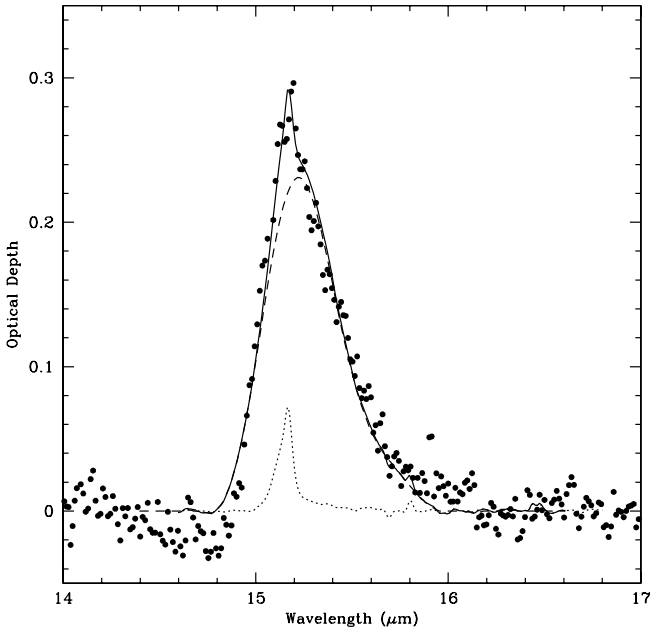

FIG. 5.—Fit (*solid line*) obtained using the laboratory profile of UV-irradiated carbon grains with a water ice cap (*dashed line*) and that of CO_2 produced after ion irradiation of CO (*dotted line*) as apolar component to CO_2 bending mode of Elias 16 (*circles*) observed with *Spitzer* by Bergin et al. (2005).

The quantitative comparison of Table 3, although not exhaustive, allows us to conclude that energetic processing of carbon grains in dense clouds is an important mechanism for the synthesis of polar CO and CO_2 solid molecules. Our conclusion relies on laboratory simulation and on an evaluation, based on considerations of general validity, of energetic processing and of the amount of carbon grains in dense clouds. Our model would benefit from further laboratory simulation of energetic processing of carbon grains with water ice mixtures containing species such as CO and oxygen. As one can see from equation (10), similar amounts of CO and CO_2 are expected to be produced by processing of carbon grains. This is a consequence of the experimental results obtained for our carbon grains with a water ice cap. The presence in the mantles of oxygen-bearing species such as CO and oxygen could modify the ratio $CO_2/CO \simeq 1$, increasing the production of CO_2. This aspect must be verified by dedicated experiments. Moreover, a quantitative evaluation of the contribution of the other proposed formation mechanisms of CO_2, such as oxidation of CO molecules of mantles by oxygen atoms and/or energetic processing of ices, at present lacking, would be advisable to further constrain the results of our model.

Energetic processing determines an interconnection between grains and their ice mantles in dense clouds. For carbon particles, the chemical composition of mantles is modified as a consequence of the specific composition of grains, yielding to the formation of CO and CO_2 molecules. In turn, these variations affect the properties of grains. As stressed by MPB04, if one considers the cycling of materials between dense and diffuse interstellar clouds, the formation of CO and CO_2 molecules on carbon grains represents a chemical erosion for these particles. In fact, when ice-mantled grains enter into diffuse regions, desorption of the mantles returns the carbon locked into these molecules into the gas phase. From equations (7) and (10) we estimate that, neglecting $A_{\rm th}$ as a first approximation, energetic processing converts about 8% of the carbon of carbonaceous particles to CO and CO_2 during a dense cloud timescale. Considering 10 cycles of particles between the two environments during their lifetime of 5×10^8 yr, the expected particle mass reduction is about 55%.

This work has been supported by Ministero dell' Istruzione, dell' Università e della Ricerca (MIUR) and Istituto Nazionale di Astrofisica (INAF) research contracts. We thank S. Inarta, N. Staiano, F. Spinella, and E. Zona for their technical assistance during laboratory measurements.

REFERENCES

Allamandola, L. J., Sandford, S. A., & Valero, G. J. 1988, Icarus, 76, 225
Baratta, G. A., Leto, G., & Palumbo, M. E. 2002, A&A, 384, 343
Bergin, E. A., Melnick, G. J., Gerakines, P. A., Neufeld, D. A., & Whittet, D. C. B. 2005, ApJ, 627, L33
Boogert, A. C. A., Hogerheijde, M. R., Ceccarelli, C., Tielens, A. G. G. M., van Dishoeck, E. F., Blake, G. A., Latter, W. B., & Motte, F. 2002, ApJ, 570, 708
Boogert, A. C. A., et al. 2004, ApJS, 154, 359
Cairns, R. B., & Samson, J. A R. 1966, J. Opt. Soc. Am., 56, 1568
Chakarov, D. V., Gleeson, M. A., & Kasemo, B. 2001, J. Chem. Phys., 115, 9477
Chiar, J. E., Adamson, A. J., Kerr, T. H., & Whittet, D. C. B. 1994, ApJ, 426, 240
———. 1995, ApJ, 455, 234
Cottin, H., Moore, M. H., & Benilan, Y. 2003, ApJ, 590, 874
Ehrenfreund, P., Boogert, A. C. A., Gerakines, P. A., Jansen, D. J., Schutte, W. A., Tielens, A. G. G. M., & van Dishoeck, E. F. 1996, A&A, 315, L341
Ehrenfreund, P., Boogert, A. C. A., Gerakines, P. A., Tielens, A. G. G. M., & van Dishoeck, E. F. 1997, A&A, 328, 649
Fournier, J., Deson, J., Vermeil, C., & Pimentel, G. C. 1979, J. Chem. Phys., 70, 5726
Gerakines, P. A., Moore, M. H., & Hudson, R. L. 2000, A&A, 357, 793
Gerakines, P. A., Schutte, W. A., & Ehrenfreund, P. 1996, A&A, 312, 289
Gerakines, P. A., Schutte, W. A., Greenberg, J. M., & van Dishoeck, E. F. 1995, A&A, 296, 810
Gerakines, P. A., et al. 1999, ApJ, 526, 1062
Gomis, O., & Strazzulla, G. 2005, Icarus, 177, 570
Greenberg, J. M. 1982, in Comets, ed. L. L. Wilkening (Tucson: Univ. Arizona Press), 131
Grim, R. J. A., & d'Hendecourt, L. B. 1986, A&A, 167, 161
Jiang, G. J., Person, W. B., & Brown, K. G. 1975, J. Chem. Phys., 62, 1201
Johnson, R. E. 1990, Energetic Charged-Particle Interactions with Atmospheres and Surfaces (Berlin: Springer)
Kerr, T. H., Adamson, A. J., & Whittet, D. C. B. 1993, MNRAS, 262, 1047
Knez, C., et al. 2005, ApJ, 635, L145
Loeffler, M. J., Baratta, G. A., Palumbo, M. E., Strazzulla, G., & Baragiola, R. A. 2005, A&A, 435, 587
Mennella, V., Baratta, G. A., Esposito, A., Ferini, G., & Pendleton, Y. J. 2003, ApJ, 587, 727
Mennella, V., Brucato, J. R., Colangeli, L., & Palumbo, P. 1999, ApJ, 524, L71
———. 2002, ApJ, 569, 531
Mennella, V., Palumbo, M. E., & Baratta, G. A. 2004, ApJ, 615, 1073 (MPB04)
Moore, M. H. 1999, in Solid Interstellar Matter: The *ISO* Revolution, ed. L. d'Hendecourt, C. Joblin, & A. Jones (Berlin: Springer), 199
Moore, M. H., Khanna, R., & Donn, B. 1991, J. Geophys. Res., 96, 17541
Munoz Caro, G., Ruiterkam, R., Schutte, W. A., Greenberg, J. M., & Mennella, V. 2001, A&A, 367, 347
Nummelin, A., Whittet, D. C. B., Gibb, E. L., Gerakines, P. A., & Chiar, J. E. 2001, ApJ, 558, 185
Palumbo, M. E., & Baratta, G. A. 2000, A&A, 361, 298
Palumbo, M. E., Baratta, G. A., Brucato, J. R., Castorina, C., Satorre, M. A., & Strazzulla, G. 1998, A&A, 334, 247
Palumbo, M. E., & Strazzulla, G. 1993, A&A, 269, 568
Pendleton, Y. J., & Allamandola, L. J. 2002, ApJS, 138, 75
Pontoppidan, K. M., et al. 2003, A&A, 408, 981
———. 2005, in IAU Symp. 231, Astrochemistry Throughout the Universe: Recent Successes and Current Challenges, ed. D. C. Lis, G. A. Blake, & E. Herbst (Cambridge: Cambridge Univ. Press), 114
Roser, J. E., Vidali, G., Manicò, G., & Pirronello, V. 2001, ApJ, 555, L61
Sandford, S. A., & Allamandola, L. J. 1990, Icarus, 87, 188
Sandford, S. A., Allamandola, L. J., Tielens, A. G. G. M., & Valero, G. J. 1988, ApJ, 329, 498
Shuping, R. Y., Snow, T. P., Chiar, J. E., & Kerr, T. 2000, ApJ, 529, 932
Teixeira, T. C., Emerson, J. P., & Palumbo, M. E. 1998, A&A, 330, 711
van Broekhuizen, F. A., Groot, I. M. N., Fraser, H. J., van Dishoeck, E. F., & Schlemmer, S. 2006, A&A, in press (astro-ph/0511815)
Watanabe, N., & Kouchi, A. 2002, ApJ, 567, 651
Westley, M. S., Baragiola, R. A., Johnson, R. E., & Baratta, G. A. 1995, Planet. Space Sci., 43, 1311
Whittet, D. C. B., et al. 1996, ApJ, 458, 363
———. 1998, ApJ, 498, L159
Yamada, H., & Person, W. B. 1964, J. Chem. Phys., 41, 2478